(Invited) Spatiotemporal soliton stability in multimode fibers: a Hamiltonian approach

Pedro Parra-Rivas, Yifan Sun, Stefan Wabnitz

[a]Dipartimento di Ingegneria dell'Informazione, Elettronica e Telecomunicazioni,Sapienza Universita di Roma, via Eudossiana 18, Roma, 00184, Italy

Abstract

We introduce a Hamiltonian approach to study the stability of three-dimensional spatiotemporal solitons in graded-index multimode optical fibers. Nonlinear light bullet propagation in these fibers can be described by means of a Gross-Pitaevskii equation with a two-dimensional parabolic potential. We apply a variational approach, based on the Ritz optimization method, and compare its predictions with extensive numerical simulations. We analytically find that, in fibers with a pure Kerr self-focusing non-linearity, spatiotemporal solitons are stable for low energies, in perfect agreement with numerical simulations. However, above a certain energy threshold, simulations reveal that the spatiotemporal solitons undergo a wave collapse, which is not captured by the variational approach.

Keywords: Light bullets, Spatiotemporal solitons, multimode fibers, Gross-Pitaevskii equation, variational approach

1. Introduction

Since the seminal paper by Zabuski and Kruskal that coined the word of soliton in 1965 [1], the emergence and dynamics of solitons in different domains of science and technology continue to attract tremendous attention. Solitons or solitary waves are localized in time or space, which propagate without suffering any shape modification. Solitons result from the interplay between linear and nonlinear processes, which acting separately would cause the wave to decay. Solitary waves arise in a plethora of different natural contexts, including hydrodynamics, plasma and condensed matter physics, biology, and nonlinear optics, to cite a few [2, 3, 4]. In the optics context, solitons are particle-like waves which may emerge in nonlinear media owing to a balance between dispersive or diffractive effects and nonlinear pulse confinement in either time or space, leading to temporal or spatial solitons, respectively [5]. Nonlinearity-induced light confinement is due to the dependence of the refractive index upon intensity of light (optical Kerr effect), which yields spatial self-(de)focusing or temporal self-phase modulation. In nonlinear dispersive media, such as single-mode optical fibers, self-phase modulation counteracts temporal broadening due to anomalous dispersion, leading to the formation of temporal solitons along the propagation direction of light. In contrast, spatial solitons form through a balance between natural diffraction-induced spreading on the one hand, and spatial self-focusing on the other hand, and form in transverse plane with respect to the propagation direction. Notably, spatial and temporal effects can couple and act simultaneously, so that dispersion and diffraction counteract Kerr nonlinearity at once, leading to light confinement in space-time. This originates the formation of a large variety of coherent spatiotemporal states, such as spatiotemporal solitons (STSs), also known as light bullets [6].

Unfortunately, fundamental Kerr STSs (i.e., solitons not carrying vorticity) are subject to a propagation instability in more than one dimension, leading to spatiotemporal *wave collapse* [6, 7, 8]. Wave collapse is a fundamental phenomenon in the context of nonlinear waves: it occurs whenever strong wave compression leads to a catastrophic blow-up of its amplitude after a finite propagation distance [7, 8]. The compression suffered by the wave needs two or more dimensions to be strong enough in order to generate the collapse. Therefore, it is absent in 1D geometries.

Email addresses: `pedro.parra-rivas@uniroma1.it` (Pedro Parra-Rivas), `yifan.sun@uniroma1.it` (Yifan Sun)

This phenomenon not only arises in nonlinear optics [9], but it also appears in different contexts, ranging from Bose-Einstein condensates (BECs) to astrophysics [10, 11, 12]. A central challenge in the scientific community remains open: namely, finding robust mechanisms which may be able to arrest the destructive wave collapse mechanisms.

In this work, we study the formation and stability of three-dimensional (3D) STSs in the context of nonlinear multimode fiber optics. Specifically, we consider the formation of STSs in fibers with a parabolic decrease of the refractive index in the transverse radial coordinate, when moving away from the center of the core [13, 14]. These fibers are known as graded-index (GRIN) fibers [15]: the parabolic refractive index variation permits to cancel, to first order, the effects of modal dispersion. In addition, the parabolic refractive index profile acts as a spatial guiding potential, which may arrest spatiotemporal wave collapse, as experimentally demonstrated by Renninger and Wise [16].

The variational approach (VA) permits to compute approximate STS solutions; moreover, it may also lead to assessing their propagation stability, by exploiting different criteria. Most of the time, the VA is based on a Lagrangian description of nonlinear wave propagation [13, 14]. In this work, we introduce a different VA, based on the Hamiltonian formulation. In this way, we find static solutions, and determine their stability by using the Lyapunov theory. Moreover, we test our findings by performing full 3D numerical simulations of the original model, and find that analytical predictions match well with numerical results for low values of STS energy. However, when the STS energy grows larger, this agreement worsens, until eventually the STSs undergo a full collapse, which is not predicted by the analytical theory.

This paper is organized as follows. In Section 2 we present the model that we will use in our analysis. After that, in Section 3 we introduce Lagrangian and Hamiltonian formulations of the model, and the Ritz optimization method. In Section 4 we obtain, by means of a Hamiltonian formulation, a reduced dynamical system containing the effective dynamics of the STSs; In Section 5 we analyze their stability. In Section 6 we test our analytical results by performing full 3D numerical simulations. Finally, in Section 7 we present our discussion or the results, and draw our conclusions.

2. The Gross-Pitaevskii equation describing graded-index multimode fibers

Electromagnetic waves propagating in GRIN waveguides can be described by the dimensionless 3D+1 Gross-Pitaevskii equation (GPE) [15]

$$\partial_z u = \frac{i}{2}\nabla_\perp^2 u + i\frac{\delta}{2}\partial_t^2 u + i\frac{\rho}{2}(x^2+y^2)u + i\nu|u|^2 u, \tag{1}$$

where $u = u(x, y, t, z)$ represents the normalized electric field component of the wave propagating along the z-direction, $\nabla_\perp^2 \equiv \partial_x^2 + \partial_y^2$ represents material diffraction, ∂_t^2 corresponds to the material group velocity dispersion (GVD), with the coefficient $\delta = \pm 1$ for anomalous/normal dispersion, $\nu = \pm 1$ for self-focusing/self-defocusing Kerr nonlinearity; $\rho(x^2 + y^2)/2$ is a 2D parabolic potential, describing the transverse spatial profile of the refractive index. Here, $\rho = -1$ ($\rho = 1$) is chosen for guiding (antiguiding) materials. The same equation can be used in the context of BECs in order to describe nearly 1D condensates, with a cigar-shaped trapping potential ($\rho < 0$) if we change the z coordinate by t [17, 18]. In this context, $\nu = 1$ models a self-attractive nonlinearity [4].

3. Variational formulation of the Gross-Pitaevskii equation and the Ritz optimization method

Equation (1) possesses the Lagrangian density

$$\mathcal{L} = -\frac{1}{2}\left(|u_x|^2 + |u_y|^2\right) - \frac{\delta}{2}|u_t|^2 + \frac{\nu}{2}|u|^4 + \frac{\rho}{2}(x^2+y^2)|u|^2 + \frac{i}{2}\left(u^* u_z - u u_z^*\right), \tag{2}$$

where we have rewritten the derivatives as $u_\xi \equiv \partial_\xi u$, with ξ being any variable x, y, z and t. This Lagrangian density contains all relevant information about the dynamics of the solutions to Eq. (1), including its conservation laws [19]. By defining the generalized field momenta $\mathcal{P} \equiv \partial_{u_z^*}\mathcal{L} = -iu/2$ and $\mathcal{P}^* \equiv \partial_{u_z}\mathcal{L} = iu^*/2$, our system can also be described by using the Hamiltonian density, which is obtained from the Legendre transform $\mathcal{H} = \mathcal{P}u_z^* + \mathcal{P}^* u_z - \mathcal{L}$, namely

$$\mathcal{H} = \frac{1}{2}\left(|u_x|^2 + |u_y|^2\right) + \frac{\delta}{2}|u_t|^2 - \frac{\nu}{2}|u|^4 - \frac{\rho}{2}\left(x^2+y^2\right)|u|^2. \tag{3}$$

The Ritz optimization method [20, 21, 22, 23] allows us to compute approximate analytical solutions of Eq. (1) by applying the principle of least action to a parameter-dependent solution ansatz. This method was utilized to predict the existence of STSs in inhomogeneous Kerr nonlinear media in terms of the Lagrangian formulation [13, 14].

The starting point of this method is to propose an approximate ansatz solution, or trial function, which captures the main features and shape of the state that we want to compute. This solution ansatz has the form $u = u[x, y, t; q(z)]$, and depends on z through a number of parameters $q(z) = \{q_1(z), \cdots, q_n(z)\}$,. These parameters are the generalized coordinates of the system. Next, we calculate the effective Lagrangian function, defined as

$$L[q(z)] \equiv \int_{\mathbb{R}^3} \mathcal{L}\{u, u_t^2, \nabla_\perp^2; u[x, y, t, q(z)]\} dxdydt. \tag{4}$$

The effective Hamiltonian is then obtained through the Legendre transform

$$H = \sum_{m=1}^{n} p_m \dot{q}_m - L \tag{5}$$

or directly from Eq. (3), that is

$$H[q(z), p(z)] \equiv \int_{\mathbb{R}^3} \mathcal{H}\{u, u_t^2, \nabla_\perp^2; u[x, y, t, q(z)]\} dxdydt, \tag{6}$$

where $p(z) = \{p_1, \cdots, p_n\}$ are the generalized momenta, defined as $p_m = \partial L / \partial \dot{q}_m$. After that, we study the dynamics emerging from the Hamiltonian equations of motion

$$\dot{q}_m = \frac{\partial H}{\partial p_m}, \qquad \dot{p}_m = -\frac{\partial H}{\partial q_m}, \qquad m = 1, \cdots, n \tag{7}$$

where $\dot{q} \equiv dq/dz$, and rebuild the desired solution through the initial ansatz.

4. Effective dynamics reduction in the Hamiltonian formalism

In order to study the formation of STSs, following [13, 14], we consider the ansatz

$$u(z, x, y, t) \equiv v[x, y, t; q_A(z)] \exp\left(iC[x, y, t; q_B(z)]\right), \tag{8}$$

with

$$v[x, y, t; q_A(z)] = A \operatorname{sech}(\eta(z)t) \exp\left(-\frac{x^2 + y^2}{2a(z)^2}\right), \tag{9}$$

and

$$C[x, y, t; q_B(z)] \equiv t^2\theta(z) + \left(x^2 + y^2\right)\alpha(z) + \phi(z), \tag{10}$$

where $q(z) = \{q_A(z), q_B(z)\}$, $q_A = \{A(z), a(z)\}$, and $q_B = \{\theta(z), \alpha(z), \phi(z)\}$. The different parameters correspond to the width of the spatial Gaussian profile $a > 0$, the inverse of the temporal width $\eta > 0$, the amplitude of the pulse $A > 0$, the spatial chirp α, the temporal chirp θ, and the phase ϕ, respectively. By using the definition of the pulse energy

$$E \equiv \int_{\mathbb{R}^3} |u(x, y, t)|^2 dxdydt = \int_{\mathbb{R}^3} v(x, y, t)^2 dxdydt, \tag{11}$$

we obtain that

$$A = \sqrt{\frac{\eta E}{2\pi a^2}}, \tag{12}$$

so that we can make our ansatz [i.e., Eq. (9)] energy dependent. In this way, the pulse energy becomes the most important control parameter for the STS solutions. Our ansatz leads to the Lagrangian

$$L(z) = -E\left[\phi_z + \frac{\pi^2\theta_z}{12\eta^2} + a^2\alpha_z + \frac{\delta}{6}\eta^2 + \frac{\pi^2\delta\theta^2}{6\eta^2} + \frac{a^2}{2}(4\alpha^2 - \rho) + \frac{1}{2a^2}\left(1 - \frac{\nu E\eta}{6\pi}\right)\right], \tag{13}$$

where $q(z) = \{\eta(z), a(z), \theta(z), \alpha(z), \phi(z)\}$. Here we want to follow the Hamiltonian formalism: therefore, we need to introduce the generalized momenta $p = (p_\eta, p_a, p_\theta, p_\alpha, p_\phi)$, canonically conjugate of $q = (\eta, a, \theta, \alpha, \phi)$:

$$p_\eta = \frac{\partial L}{\partial \dot{\eta}}, \qquad p_a = \frac{\partial L}{\partial \dot{a}}, \qquad p_\theta = \frac{\partial L}{\partial \dot{\theta}}, \qquad p_\alpha = \frac{\partial L}{\partial \dot{\alpha}}, \qquad p_\phi = \frac{\partial L}{\partial \dot{\phi}}. \tag{14}$$

By using the Lagrangian function defined by Eq. (13), the momenta read as

$$p_\eta = 0, \qquad p_a = 0, \qquad p_\theta = -\frac{E\pi^2}{12\eta^2}, \qquad p_\alpha = -Ea^2, \qquad p_\phi = -E. \tag{15}$$

As previously mentioned, the Hamiltonian can be computed by considering two different approaches. One of them uses Eq. (6) with the Hamiltonian density (3) and the chirp-dependent ansatz (8); whereas the second approach applies the Legendre transform (5). In any case, we obtain the effective Hamiltonian

$$H = E\left[\frac{\delta\eta^2}{6} + \frac{\pi^2\delta\theta^2}{6\eta^2} + \frac{a^2}{2}(4\alpha^2 - \rho) + \frac{1}{2a^2}\left(1 - \frac{E\nu\eta}{6\pi}\right)\right], \tag{16}$$

which, written in terms of the generalized momenta, reads as

$$H(\theta, \alpha, p_\theta, p_\alpha) = -E\left[\frac{\delta E\pi^2}{72p_\theta} + \frac{2\delta\theta^2 p_\theta}{E} + \frac{p_\alpha}{2E}(4\alpha^2 - \rho) + \frac{E}{2p_\alpha}\left(1 - \frac{E\nu}{6}\sqrt{-\frac{E}{12p_\theta}}\right)\right], \tag{17}$$

where we have kept E as control parameter, instead of replacing it by $-p_\phi$. In this case, the Hamiltonian equations of motion [see Eqs. (7)] describing the dynamics of the system become

$$\frac{dp_\theta}{dz} = -\frac{\partial H}{\partial \theta} = 4\delta\theta p_\theta, \tag{18}$$

$$\frac{dp_\alpha}{dz} = -\frac{\partial H}{\partial \alpha} = 4\alpha p_\alpha, \tag{19}$$

$$\frac{d\theta}{dz} = \frac{\partial H}{\partial p_\theta} = -2\delta\theta^2 + \frac{E^2}{72p_\theta^2}\left(\delta\pi^2 + \frac{E^2\nu}{4p_\alpha}\sqrt{-\frac{12p_\theta}{E}}\right), \tag{20}$$

$$\frac{d\alpha}{dz} = \frac{\partial H}{\partial p_\alpha} = \frac{1}{2}(\rho - 4\alpha^2) + \frac{E^2}{2p_\alpha^2}\left(1 - \frac{E\nu}{6\pi}\sqrt{-\frac{E\pi^2}{12p_\theta}}\right). \tag{21}$$

In this way, we could reduce the original Eq. (1) to a 4D dynamical system, defined in the phase space $(p_\theta, p_\alpha, \theta, \alpha)$, which contains all information about the dynamics of the STS ansatz (8). Note that $\frac{dp_\phi}{dz} = -\frac{\partial H}{\partial \phi} = 0$, which implies that p_ϕ remains constant during the propagation, and therefore E is conserved.

5. Spatiotemporal soliton solutions

In the Hamiltonian formulation, the steady-state solutions or STSs are represented as the equilibria of the reduced system. These are obtained from the nullity of the gradient of H evaluated at $q = q_e = (\theta_e, \alpha_e, p_\theta^e, p_\alpha^e)$ [19], namely

$$\mathcal{D}H|_{q_e} \equiv (\partial_\theta H, \partial_\alpha H, \partial_{p_\theta} H, \partial_{p_\alpha} H)_{(q_e, p_e)} = 0. \tag{22}$$

The first two conditions yield the nullity of the temporal and spatial chirp ($\theta_e = \alpha_e = 0$), which means that our STS must be chirp-free. These, once combined with Eqs. (20) and Eqs. (21), lead to

$$\delta\pi^2 + \frac{E^2\nu}{4p_\alpha^e}\sqrt{-\frac{12p_\theta^e}{E}} = 0, \qquad \frac{\rho}{2} + \frac{E^2}{2p_\alpha^{e\,2}}\left(1 - \frac{E\nu}{6\pi}\sqrt{-\frac{E\pi^2}{12p_\theta^e}}\right) = 0, \tag{23}$$

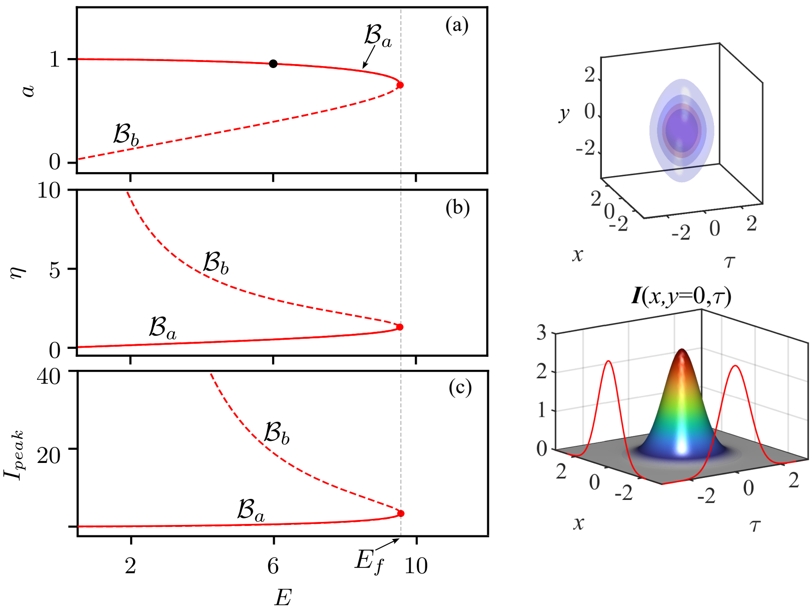

Figure 1: Bifurcation diagrams for the STS states as a function of E. Left column: self-focusing/anomalous GVD. (a) shows the width of the STS ($a = a_e$) as a function of E, (b) shows the inverse of the temporal width $\eta = \eta_e$, (c) the STS peak intensity I_{peak}. The branch of solutions $\mathcal{B}_a$ is plotted in solid, while $\mathcal{B}_b$ uses a dashed line. The black dot (●) in panel (a) corresponds to the STS shown on the right.

respectively. By inserting the expressions for p_α and p_θ in the previous equations, we obtain

$$\frac{E\nu}{a_e^2} - 4\pi\delta\eta_e = 0, \qquad E\nu\eta_e - 6\pi(1+\rho a_e^4) = 0, \tag{24}$$

providing that $a_e > 0$. By combining these expressions, one finally obtains that the static soliton parameters satisfy

$$E = 2\pi a_e\sqrt{6\delta(1+\rho a_e^4)} \tag{25}$$

$$\eta_e = \frac{E\nu}{4\pi\delta a_e^2} = \frac{\nu}{2\delta a_e}\sqrt{6\delta(1+\rho a_e^4)}, \tag{26}$$

and

$$I_{peak} = |A|^2 = \frac{E\eta}{2\pi a^2} = \frac{3\nu}{a_e^2}(1+\rho a_e^4). \tag{27}$$

From Eqs. (25) and (26), we find that $\delta(1+\rho a_e^4) > 0$. When $1+\rho a_e^4 = 0$ (i.e., $a_e^4 = -1/\rho$), E and η_e become zero. This means that as $E \to 0$, the temporal width of the state $\eta_e^{-1} \to \infty$, and the STS reduces to the continuous-wave solution of the system. Furthermore, from Eq. (26) we can see that δ and ν must have the same sign, in order for η_e to be positive. Equation (25) can also be written in the form

$$\rho a_e^6 + a_e^2 - \frac{1}{6\delta}\left(\frac{E}{2\pi}\right)^2 = 0, \tag{28}$$

and it may have one or two positive real roots, depending on the signs of ν, δ, and ρ. In what follows, we will consider *guiding media*: therefore, we may take $\rho < 0$. Furthermore, we focus on the case of a self-focusing nonlinear material ($\nu = 1$) with anomalous GVD ($\delta = 1$). In this case, Eqs. (25), (26), and (27) simplify to

$$E = 2\pi a_e\sqrt{6(1+\rho a_e^4)}, \qquad \eta_e = \frac{1}{2a_e}\sqrt{6(1+\rho a_e^4)}, \qquad I_{peak} = \frac{3}{a_e^2}(1+\rho a_e^4).$$

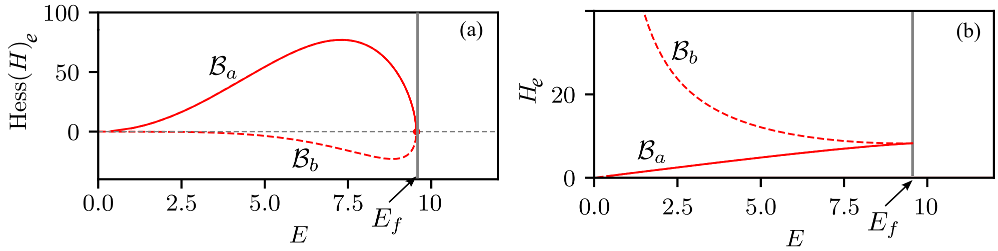

Figure 2: Lyapunov stability of STSs. Panel (a) shows the dependence of the Hessian of H with E for the self-focusing/anomalous GVD regime, where we have multiply the vertical axis by a factor 10^{-3}. Panel (b) shows the H_e versus E diagram.

Figures 1(a)-(c) show the modification of these quantities as a function of E for $\rho = -1$. In this regime, Eq. (28) has, for a fixed value of E, two real solutions, which lead to the solution branches $\mathcal{B}_a$ (solid red line), and $\mathcal{B}_b$ (dashed red line). These two solution branches coexist between $E = E_0 \equiv 0$ and the fold, or turning point, which takes place at $E = E_f$ (see red dots in Fig. 1). The fold position can be calculated analytically, by solving the equation $dE/da_e = 0$, which leads to $1 + 3\rho a_e^4 = 0$, providing that $1 + \rho a_e^4 > 0$. The solution of this equation yields the fold parameters

$$a_f = (-3\rho)^{-1/4}, \qquad \eta_f = (-3\rho)^{1/4}, \qquad E_f = 4\pi a_f, \qquad I_f = \frac{2}{a_f^2}.$$

In the right column of Fig. 1 we show an example of a stable STS, reconstructed by using Eq. (8) for $E = 8$ (see top figure). To represent the bullets, we plot iso-surfaces for different fixed-intensity values. The bottom panel represents the wave-function intensity cross-sections at the plane $t = 0$, i.e. $I(x, y = 0, \tau)$. Increasing E, the STSs on $\mathcal{B}_a$ decrease their spatial and temporal width, while simultaneously increasing their intensity (i.e., I_{peak}).

6. Lyapunov stability criterion for light bullets

An important question that one could ask at this stage is if the STS states are stable or not. To answer this, different methods can be considered, including the Vakhitov-Kolokolov criteria [24], or the spectral stability [14]. Here, we consider a different approach to determine STS stability, based on Eq. (17). The Hamiltonian provides information about the stability of the fixed points in terms of the Lyapunov stability criterion [25, 26]. The Lyapunov stability criterion establishes that if an equilibrium q_e minimizes (maximizes) H, such a state is stable (unstable). When evaluated at the STS equilibria q_e, the Hamiltonian reads

$$H_e \equiv H(0, 0, p_\theta^e, p_\alpha^e) = -E\left[\frac{\delta E\pi^2}{72 p_\theta^e} - \frac{\rho p_\alpha^e}{2E} + \frac{E}{2p_\alpha^e}\left(1 - \frac{E\nu}{6}\sqrt{-\frac{E}{12 p_\theta^e}}\right)\right], \tag{29}$$

or, in terms of the generalized coordinates,

$$H_e \equiv H(q_e) = E\left[\frac{\delta \eta_e^2}{6} - \frac{\rho a_e^2}{2} + \frac{1}{2a^2}\left(1 - \frac{E\nu\eta_e}{6\pi}\right)\right]. \tag{30}$$

The way of determining if H_e is a maximum or a minimum is by studying the determinant of the Hessian matrix associated with H, once it is evaluated at q_e. By definition, the components of the Hessian matrix of H, evaluated at q_e, read as

$$\mathcal{D}^2 H(q_e)_{(i,j)} \equiv \left(\frac{\partial^2 H}{\partial q_i \partial q_j}\right)(q_e), \tag{31}$$

where the subindex $i, j = 1, \cdots, 4$ scans the four STSs parameters $(q_1, q_2, q_3, q_4) = (\eta, a, \theta, \alpha)$. The determinant of this matrix, known as the Hessian of H, reduces to

$$\text{Hess}(H)_e \equiv \det\left(\mathcal{D}^2 H(q_e)\right) = -\frac{\delta E^4\left(12\delta\rho\pi^2 a_e^6 + 6\delta\pi a_e^2(\eta_e \nu E - 6\pi) + E^2\right)}{27 a_e^4 \eta_e^2}. \tag{32}$$

Now, if $\text{Hess}(H)_e > 0$, H reaches the minimum value $H_e = H(q_e)$ at $q = q_e$, and thus q_e is a stable equilibrium. However, when $\text{Hess}(H)_e < 0$, H has a maximum at $q = q_e$ which is therefore unstable. The transition between these two situations occurs when $\text{Hess}(H)_e = 0$, which leads to the instability threshold.

Figure 2(a) shows $\text{Hess}(H)_e$ as a function of E for the case of a self-focusing/anomalous GVD regime. The solid red part of this curve (i.e., $\text{Hess}(H)_e > 0$) corresponds to the stable STS branch $\mathcal{B}_a$, which extends from $a = 0$ to $a = a_f$ [see Fig. 1(a)]. The dashed curve ($\text{Hess}(H)_e < 0$) corresponds to $\mathcal{B}_b$, and the condition $\text{Hess}(H)_e = 0$ is associated with the fold point occurring at $E = E_f$. In Fig. 2(b) we plot the H_e versus E diagram: such a diagram was also used in other works, in order to determine soliton stability [27]. This diagram confirms what was already predicted through the diagram shown in Fig. 2(a): the STS equilibria on $\mathcal{B}_a$ minimize H, and therefore, correspond to stable STSs, while those on $\mathcal{B}_b$ are unstable, as they maximize H. The cusp of this graph corresponds to the position of the fold point which is shown in Figs. 1(a)-(c) and in Fig. 2(a).

7. Full three-dimensional numerical simulations

The aim of this section is to compare the theoretical results obtained by the Hamiltonian approach, with direct numerical simulations of the original GPE (1). To solve this initial value problem, we take as the initial condition the approximate variational solution defined by Eq. (8) with the parameters corresponding to equilibria of the effective dynamical theory. To do so, we utilize a pseudo-spectral split-step algorithm [28] where the differential part of Eq. (1) is evaluated via the fast Fourier transform method.

The z-evolutions of the initial stable chirp-free STS solutions are shown in Figs. 3(a)-(c) for $E = 6$. Panel (a) shows the evolution of the STS intensity with z at its center (see blue curve), as well as the analytically predicted intensity value (dashed gray line). The evolution of the STS intensity is not constant, but it fluctuates around a value that is a bit larger than what is predicted by the Hamiltonian approach. These fluctuations are depicted in more detail in Fig. 3(b) for the interval $z \in (950, 1000)$. The evolution of the STS shape is illustrated every propagation distance $\Delta z = 10$ in Fig. 3(c), by considering two iso-surfaces at intensities $I_1 = 0.5$ and $I_2 = 0.1$, respectively. The discrepancy between the analytical intensity value and the average intensity, computed from the full numerical simulations in the interval $z \in (0, 1000)$ is shown in Fig. 3(d), by using a red line and blue circles, respectively. The agreement is quite good for relatively low STS energy values, or $E < 6$, but it worsens with increasing E. Numerical STSs fluctuate more heavily as E increases. Eventually, for energy values above $E \approx 8.5$, the STS undergoes a wave collapse (see vertical blue lines), much before the threshold at $E = E_f$ which is predicted by the theory (see red dot).

Hence, although it is not predicted by the VA, for high values of energy E the self-focusing of the field leads to its collapse in the GPE. To our knowledge, this disagreement between theory and numerical results was not yet described in the literature. Wave collapse might be arrested by including higher-order self-defocusing nonlinearities, such as quintic-order terms, or by considering high-order dispersive effects. However, a confirmation of these scenarios requires further investigations.

8. Discussions and conclusions

In this work, we have presented a systematic analysis of three-dimensional spatiotemporal solitons, also known as light bullets, appearing in the 3D+1 GPE with a 2D parabolic potential, which can be used to describe light propagation in GRIN multimode optical fibers [13, 14, 29, 15, 16]. The GPE possesses a Lagrangian and a Hamiltonian structure, that we have introduced in Section 3. There, we showed that analytical approximations for soliton solutions can be computed through the Ritz optimization approach, by considering an adequate parameter-dependent solution ansatz. This approach, based on the variational method, allows for reducing the GPE to a low-dimensional dynamical system, which describes the effective dynamics of spatiotemporal localized solutions. Following a Hamiltonian approach, we have obtained such a system in Section 4, by considering the anomalous GVD (or self-focusing) regime. The corresponding equilibria of such a system correspond to two families of STSs, $\mathcal{B}_a$ and $\mathcal{B}_b$, which coexist for the same parameter regime (see Section 5). In Section 6 we have determined the STS stability by using the Lyapunov criterion, based on the H_e vs. E dependence. Finally, in Section 7 we have tested our analytical predictions by performing advanced numerical simulations of the initial value problem associated with the full 3D+1 GPE (1). By doing so, we demonstrated that, for low E, the agreement between the VA and numerical simulations is excellent, as depicted

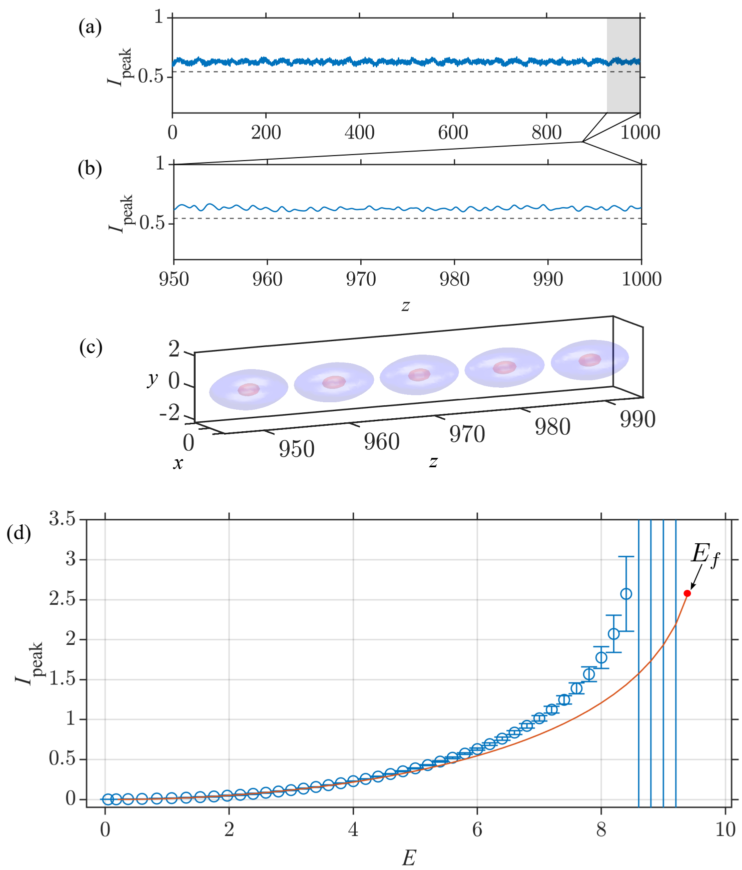

Figure 3: Evolution along z of a stable LS for $E = 6$. Panel (a) shows the variation of the intensity within the whole propagation distance. Panel (b) shows a close-up view of (a) for the interval $z \in [950, 1000]$. Panel (c) shows the evolution of the STSs along the interval shown in (b) by plotting two iso-surfaces at $I_1 = 0.5$ (red), and $I_2 = 0.1$ (blue). The dashed gray straight lines in (a) and (b) represent the theoretical value of the STS intensity. (d) Evolution of peak intensity of stable STSs with the energy E. The red line shows the analytical value, while the blue circles and the error bars represent the average intensity value and the standard deviation for stable states, respectively, which are obtained from full 3D numerical simulations.

in Figs. 3. When increasing E, however, a disagreement appears, and STSs suffer a wave collapse in an interval of energies where they should remain stable, according to the theoretical analysis. The disagreement between theory and numerical simulations was left unnoticed in previous works, where the studies either involved a single energy value, or considered scenarios restricted to soliton solutions with radial symmetry [13, 14, 29].

In perspective, further work is necessary in order to explore different mechanisms that can be able of arresting the wave collapse. One of the possible paths to follow is to consider higher-order nonlinearities, which may come into play for very high E [30, 31]. In particular, one may conside self-defocusing quintic nonlinearities, which could counteract the self-focusing Kerr nonlinearity that was studied here. Quintic nonlinear effects have been discussed in Ref. [32], but in the absence of a parabolic potential. Hence, our hypothetical stabilization scenario remains so far unexplored. A different route for stabilizing spatiotemporal solitons may involve the inclusion of high-order dispersion terms.

This work was supported by European Research Council (740355), Marie Sklodowska-Curie Actions (101023717, 101064614), Ministero dell'Istruzione, dell'Università e della Ricerca (R18SPB8227).

References

[1] N. J. Zabusky, M. D. Kruskal, Interaction of "solitons" in a collisionless plasma and the recurrence of initial states, Phys. Rev. Lett. 15 (1965) 240–243. doi:10.1103/PhysRevLett.15.240.

URL https://link.aps.org/doi/10.1103/PhysRevLett.15.240

[2] T. Dauxois, M. Peyrard, Physics of Solitons, Cambridge University Press, 2006, google-Books-ID: YKe1UZc_Qo8C.

[3] Y. V. Kartashov, G. E. Astrakharchik, B. A. Malomed, L. Torner, Frontiers in multidimensional self-trapping of nonlinear fields and matter, Nature Reviews Physics 1 (3) (2019) 185–197, number: 3 Publisher: Nature Publishing Group. doi:10.1038/s42254-019-0025-7.
URL https://www.nature.com/articles/s42254-019-0025-7

[4] B. A. Malomed, Multidimensional SolitonsPublisher: AIP Publishing LLCAIP PublishingMelville, New York. doi:10.1063/9780735425118.
URL https://aip.scitation.org/doi/abs/10.1063/9780735425118

[5] Y. S. Kivshar, G. P. Agrawal, Y. S. Kivshar, Optical Solitons: From Fibers to Photonic Crystals, Amsterdam ; Boston, 2003.

[6] Y. Silberberg, Collapse of optical pulses, Optics Letters 15 (22) (1990) 1282–1284, publisher: Optica Publishing Group. doi:10.1364/OL.15.001282.
URL https://opg.optica.org/ol/abstract.cfm?uri=ol-15-22-1282

[7] L. Bergé, Wave collapse in physics: principles and applications to light and plasma waves, Physics Reports 303 (5) (1998) 259–370. doi:10.1016/S0370-1573(97)00092-6.
URL https://www.sciencedirect.com/science/article/pii/S0370157397000926

[8] O. Bang, W. Krolikowski, J. Wyller, J. J. Rasmussen, Collapse arrest and soliton stabilization in nonlocal nonlinear media, Physical Review E 66 (4) (2002) 046619, publisher: American Physical Society. doi:10.1103/PhysRevE.66.046619.
URL https://link.aps.org/doi/10.1103/PhysRevE.66.046619

[9] E. Garmire, R. Y. Chiao, C. H. Townes, Dynamics and Characteristics of the Self-Trapping of Intense Light Beams, Physical Review Letters 16 (9) (1966) 347–349, publisher: American Physical Society. doi:10.1103/PhysRevLett.16.347.
URL https://link.aps.org/doi/10.1103/PhysRevLett.16.347

[10] C. A. Sackett, J. M. Gerton, M. Welling, R. G. Hulet, Measurements of Collective Collapse in a Bose-Einstein Condensate with Attractive Interactions, Physical Review Letters 82 (5) (1999) 876–879, publisher: American Physical Society. doi:10.1103/PhysRevLett.82.876.
URL https://link.aps.org/doi/10.1103/PhysRevLett.82.876

[11] A. Y. Wong, P. Y. Cheung, Three-Dimensional Self-Collapse of Langmuir Waves, Physical Review Letters 52 (14) (1984) 1222–1225, publisher: American Physical Society. doi:10.1103/PhysRevLett.52.1222.
URL https://link.aps.org/doi/10.1103/PhysRevLett.52.1222

[12] Black Holes, in: Black Holes, White Dwarfs, and Neutron Stars, John Wiley & Sons, Ltd, 1983, pp. 335–369, section: 12 _eprint: https://onlinelibrary.wiley.com/doi/pdf/10.1002/9783527617661.ch12. doi:10.1002/9783527617661.ch12.
URL https://onlinelibrary.wiley.com/doi/abs/10.1002/9783527617661.ch12

[13] S.-S. Yu, C.-H. Chien, Y. Lai, J. Wang, Spatio-temporal solitary pulses in graded-index materials with Kerr nonlinearity, Optics Communications 119 (1) (1995) 167–170. doi:10.1016/0030-4018(95)00377-K.
URL https://www.sciencedirect.com/science/article/pii/003040189500377K

[14] S. Raghavan, G. P. Agrawal, Spatiotemporal solitons in inhomogeneous nonlinear media, Optics Communications 180 (4) (2000) 377–382. doi:10.1016/S0030-4018(00)00727-6.
URL https://www.sciencedirect.com/science/article/pii/S0030401800007276

[15] P. Horak, F. Poletti, Multimode Nonlinear Fibre Optics: Theory and Applications, Recent Progress in Optical Fiber Research (Jan. 2012). doi:10.5772/27489.
URL https://www.intechopen.com/books/recent-progress-in-optical-fiber-research/multimode-nonlinear-fibre-optics-theory-a

[16] W. H. Renninger, F. W. Wise, Optical solitons in graded-index multimode fibres, Nature Communications 4 (1) (2013) 1719. doi:10.1038/ncomms2739.
URL https://www.nature.com/articles/ncomms2739

[17] K. E. Strecker, G. B. Partridge, A. G. Truscott, R. G. Hulet, Formation and propagation of matter-wave soliton trains, Nature 417 (6885) (2002) 150–153, number: 6885 Publisher: Nature Publishing Group. doi:10.1038/nature747.
URL https://www.nature.com/articles/nature747

[18] B. A. Malomed, Multidimensional solitons: Well-established results and novel findings, The European Physical Journal Special Topics 225 (13) (2016) 2507–2532. doi:10.1140/epjst/e2016-60025-y.
URL https://doi.org/10.1140/epjst/e2016-60025-y

[19] R. Abraham, J. E. Marsden, Foundations of Mechanics, American Mathematical Soc., 2008.

[20] D. Anderson, M. Bonnedal, M. Lisak, Self-trapped cylindrical laser beams, The Physics of Fluids 22 (9) (1979) 1838–1840, publisher: American Institute of Physics. doi:10.1063/1.862795.
URL https://aip.scitation.org/doi/abs/10.1063/1.862795

[21] A. Bondeson, M. Lisak, D. Anderson, Soliton Perturbations: A Variational Principle for the Soliton Parameters, Physica Scripta 20 (3-4) (1979) 479. doi:10.1088/0031-8949/20/3-4/024.
URL https://dx.doi.org/10.1088/0031-8949/20/3-4/024

[22] V. M. Pérez-García, H. Michinel, J. I. Cirac, M. Lewenstein, P. Zoller, Dynamics of Bose-Einstein condensates: Variational solutions of the Gross-Pitaevskii equations, Physical Review A 56 (2) (1997) 1424–1432. doi:10.1103/PhysRevA.56.1424.

[23] B. A. Malomed, Variational methods in nonlinear fiber optics and related fields, in: Progress in Optics, Vol. 43, Elsevier, 2002, pp. 71–193. doi:10.1016/S0079-6638(02)80026-9.
URL https://linkinghub.elsevier.com/retrieve/pii/S0079663802800269

[24] N. G. Vakhitov, A. A. Kolokolov, Stationary solutions of the wave equation in a medium with nonlinearity saturation, Radiophysics and Quantum Electronics 16 (7) (1973) 783–789. doi:10.1007/BF01031343.
URL https://doi.org/10.1007/BF01031343

[25] R. Reiszig, J. LaSalle and S. Lefschetz, Stability by Liapunov's Direct Method with Applications. VII + 134 S. New York/London 1961. Academic Press. Preis geb. $ 5.50, ZAMM - Journal of Applied Mathematics and Mechanics / Zeitschrift für Angewandte Mathematik und

Mechanik 42 (10-11) (1962) 514–514, _eprint: https://onlinelibrary.wiley.com/doi/pdf/10.1002/zamm.19620421022. doi:10.1002/zamm.19620421022.
URL https://onlinelibrary.wiley.com/doi/abs/10.1002/zamm.19620421022

[26] G. Rosen, Particlelike Solutions to Nonlinear Scalar Wave Theories, Journal of Mathematical Physics 6 (8) (1965) 1269–1272, publisher: American Institute of Physics. doi:10.1063/1.1704769.
URL https://aip.scitation.org/doi/10.1063/1.1704769

[27] N. Akhmediev, A. Ankiewicz, R. Grimshaw, Hamiltonian-versus-energy diagrams in soliton theory, Physical Review E 59 (5) (1999) 6088–6096, publisher: American Physical Society. doi:10.1103/PhysRevE.59.6088.
URL https://link.aps.org/doi/10.1103/PhysRevE.59.6088

[28] G. Agrawal, Applications of Nonlinear Fiber Optics, Academic Press, 2008, google-Books-ID: HbkKQLPE8yEC.

[29] O. V. Shtyrina, M. P. Fedoruk, Y. S. Kivshar, S. K. Turitsyn, Coexistence of collapse and stable spatiotemporal solitons in multimode fibers, Physical Review A 97 (1) (2018) 013841, publisher: American Physical Society. doi:10.1103/PhysRevA.97.013841.
URL https://link.aps.org/doi/10.1103/PhysRevA.97.013841

[30] M. Karlsson, Optical beams in saturable self-focusing media, Physical Review A 46 (5) (1992) 2726–2734, publisher: American Physical Society. doi:10.1103/PhysRevA.46.2726.
URL https://link.aps.org/doi/10.1103/PhysRevA.46.2726

[31] V. I. Berezhiani, S. M. Mahajan, Large relativistic density pulses in electron-positron-ion plasmas, Physical Review E 52 (2) (1995) 1968–1979, publisher: American Physical Society. doi:10.1103/PhysRevE.52.1968.
URL https://link.aps.org/doi/10.1103/PhysRevE.52.1968

[32] V. Skarka, V. I. Berezhiani, R. Miklaszewski, Spatiotemporal soliton propagation in saturating nonlinear optical media, Physical Review E 56 (1) (1997) 1080–1087, publisher: American Physical Society. doi:10.1103/PhysRevE.56.1080.
URL https://link.aps.org/doi/10.1103/PhysRevE.56.1080